Electroreflectance spectroscopy of Si-Ge_xSi_{1-x} quantum-well structures

T. P. Pearsall
AT&T Bell Laboratories, Murray Hill, New Jersey 07974

F. H. Pollak
Department of Physics, Brooklyn College of the City University of New York, Brooklyn, New York 11210 and Center for Advanced Technology in Telecommunications, Polytechnic University, Brooklyn, New York 11201

J. C. Bean and R. Hull*
AT&T Bell Laboratories, Murray Hill, New Jersey 07974
(Received 5 August 1985)

Electroreflectance spectroscopy of Ge_xSi_{1-x} decoupled multiple-quantum-well structures grown by molecular-beam epitaxy has been used to yield confinement energy and strain shifts for the E_0 and E_1 optical transitions. The strain induced by lattice mismatch decouples the valence band at the zone center permitting resolution of the strain-split E_0 valence-band states. Confinement of electrons and holes in quantum-well states has an additional important effect on the optical transition energies for narrow (<50 Å) wells. Good quantitative agreement is obtained between experimental results and the full theoretical treatment of strain and confinement.

I. INTRODUCTION

The development of Si molecular-beam epitaxy[1-3] has opened the doorway to band-structure engineering through heterostructures formed from the strained-layer coherent epitaxy of Si and Ge.[4] Enhanced mobility in heavily doped *n*-type Ge-Si superlattices has been measured[5] and shown to result from modifications of the effective-mass tensor which are unique to indirect-gap systems.[6] Two-dimensional carrier confinement in *p*-type modulation-doped heterojunctions has been exploited in the fabrication of buried-channel heterojunction-confinement modulation-doped field-effect transistors.[7(a)] These developments suggest intriguing possibilities for the tailoring of Si properties for certain applications in very large-scale integrated (VLSI) and photonic circuits.[7(b)]

Cerdeira *et al.* have studied Ge_xSi_{1-x} multiple-quantum-well structures using resonant Raman scattering as a probe near the zone-center E_0 transition. These results show the presence of both strain[8] and quantum confinement[9] on the resonance energy. In this work we have used electroreflectance (ER) to study all the principal optical transitions in some Si-Ge_xSi_{1-x} quantum-well structures in an effort to quantify the effects of strain and quantum confinement on the transition energies. Modulation spectroscopy has proven to be a valuable tool for the investigation of quantum confinement in superlattices and quantum-well structures.[10-12]

II. EXPERIMENTAL CONDITIONS

All samples were grown by molecular-beam epitaxy (MBE) on [100]-oriented silicon substrates. Conditions were chosen such that the GeSi layers are compressed in the growth plane to match the smaller Si lattice parameter. Details of this strained-layer epitaxial process have been presented elsewhere.[4] To summarize, GeSi layers are grown at temperatures of approximately 550°C, on low-defect-density substrates, to thickness not exceeding the so-called "critical thickness" for strained-layer epitaxy. This critical thickness defines the boundary between strain-accommodated mismatch and the onset of misfit dislocation formation. Values of this parameter are given in Fig. 1. For Ge-rich alloys grown on Si substrates this thickness is less than 100 Å. Fortunately, it has been found that alloy layers are much more elastic than thin

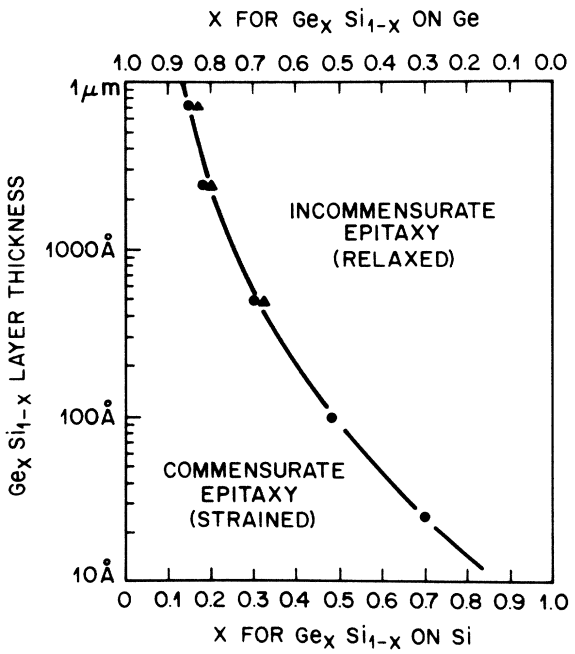

FIG. 1. Critical layer thickness for strained-layer epitaxy of GeSi on Si and Ge as a function of alloy composition.

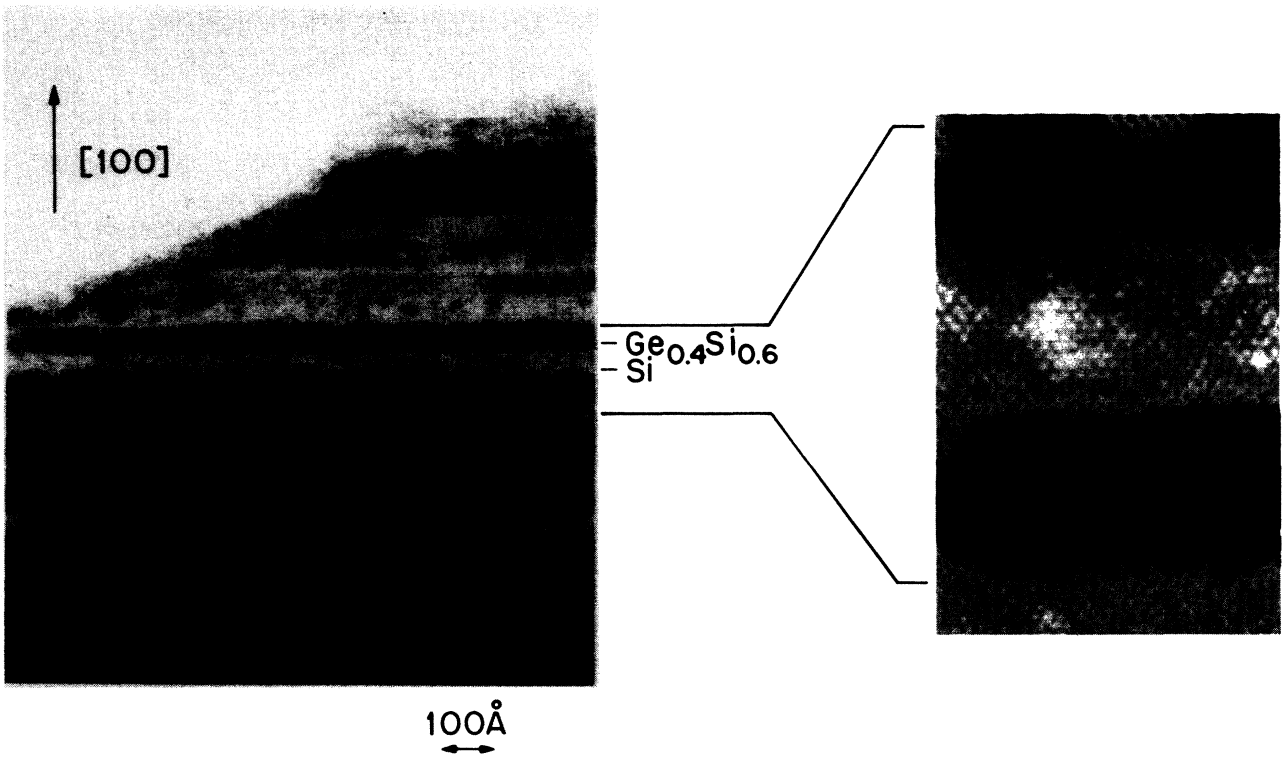

FIG. 2. Transmission electron micrographs of a typical strained-layer superlattice. Left-hand photo: cross section of entire structure. Right-hand photo: phase contrast image resolving atomic pairs. Image has been computer color enhanced to expand contrast scale.

layers.[8,9] Indeed, as long as Si layers are ≈ 3—5 times thicker than GeSi layers, the Si will retain a bulk structure. The total alloy volume can therefore be increased by stacking alternating GeSi and Si layers into superlattices.

In the MBE system,[13] superlattices can be readily produced by the rapid movement of motorized deposition shutters. Although timers were used for early experiments complex structures are now more readily grown using a personal computer (AT&T model No. 6300). Transmission electron micrographs of a typical strained-layer superlattice are shown in Fig. 2. The left-hand photo is a conventional image showing a cross section of the entire structure. Interfaces are smooth and regular with no evidence of dislocations despite the 3% lattice mismatch between the constituent layers. The right-hand micrograph was taken in a phase contrast mode in which columns of atom pairs can be resolved. This and other micrographs have been computer color enhanced in order to expand the contrast range. Results indicate that layers are compositionally uniform except for random effects in the alloy. Negligible Ge diffusion into cladding silicon layers is observed.

The modulation reflectance spectra were taken in the visible to near UV region of the optical spectrum. The optical susceptibility was modulated by an electric field applied to the sample surface via a 50-Å semitransparent Ni Schottky barrier.[14] The modulation voltage for all measurements was 4 V rms with a 2.5-V dc reverse bias. The incident radiation was produced by a 150-W xenon arc lamp. The output was filtered by a $f/4$ monochromator with 1.5- and 0.5-mm entrance and exit slits. Instrumental resolution is better than 2 nm under these conditions corresponding to ≈ 15 meV in the measured transition energies.

The optical transition energies for unstrained Ge_xSi_{1-x}

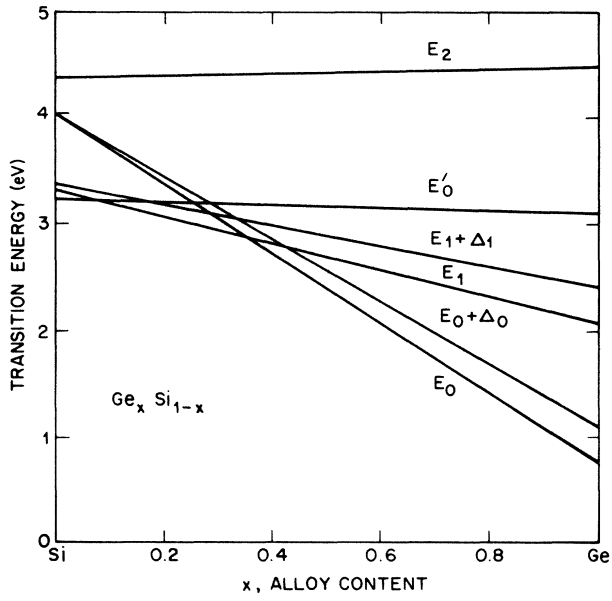

FIG. 3. Direct optical transition energies for unstrained Ge_xSi_{1-x} alloys from the data of Kline, Pollak, and Cardona (Ref. 15).

alloys measured by Kline, Pollak, and Cardona[15] are shown in Fig. 3. These range between 0.8 and 4.5 eV. Note that the E_1 and E_0' transitions at ≈ 3.3 eV are the lowest-energy optical transitions for Si. The transitions from the Ge_xSi_{1-x} alloys which occur in the range 0.8—3.0 eV are easily distinguished, therefore, from the signal from Si barrier layers. Fused silica optics were used to study the high-energy transitions, while borosilicate optics were used as a convenient filter to resolve features in the (2.0—3.0)-eV region without interference effects from second-order transmission of the grating. The photomultiplier gain was controlled by a fast electronic servo keeping the measured dc intensity constant. The modulated signal was detected using a lock-in amplifier (Princeton Applied Research, model No. 124A) and recorded directly. Spectra recorded in this manner are equivalent to the third derivative spectra of the optical dielectric function[14] in the low-field limit.

III. THE EFFECT OF STRAIN ON TRANSITION ENERGIES

A. The E_0 and $E_0+\Delta_0$ transitions

The E_0 and $E_0+\Delta_0$ optical features correspond to direct transitions from the spin-orbit-split Γ_{25}' valence-band to the Γ_2' conduction-band states.

A schematic diagram of the valence bands of both unstrained and strained Ge_xSi_{1-x} is shown in Fig. 4. The general effect of strain is to provoke a shift in both the $J=\frac{3}{2}$ and $J=\frac{1}{2}$ manifolds as well as a splitting of the doubly degenerate $J=\frac{3}{2}$ manifold:[16–18]

$$\begin{aligned}\mathscr{H}_{\text{strain}} = &-(a^c-a^v)(\epsilon_{xx}+\epsilon_{yy}+\epsilon_{zz}) \\ &-3b[(L_x^2-\tfrac{1}{3}L^2)\epsilon_{xx}+\text{c.p.}] \\ &-\sqrt{3}d[(L_xL_y+L_yL_x)\epsilon_{xy}+\text{c.p.}]\ , \end{aligned} \tag{1}$$

where ϵ_{ij} denotes components of the strain tensor, **L** is the angular momentum operator, and c.p. denotes cyclic permutation with respect to the indices x,y,z. The quantities a^c and a^v represent the shift of the conduction band (Γ_2') and valence band (Γ_{25}), respectively, due to the hydrostatic components of the strain while b and d are the tetragonal and trigonal deformation potentials, respectively.

The direction of the induced level shift and splitting are determined by the geometry of the strain and is given by Eq. (1). Our multiple quantum-well structures consist of planar layers grown along the [001] axis. Lattice mismatch between Ge_xSi_{1-x} quantum wells and the Si cladding layers produces a biaxial compressive strain in the [100] and [010] directions which is entirely taken up in the Ge_xSi_{1-x} well region. The strain in the Si cladding layers is taken to be zero because of the effect of the Si substrate which is substantially thicker than the region of strained-layer epitaxy and the fact that the Si cladding layers are much thicker than the alloy quantum wells.

The [001] direction, being unconstrained, is free of stress. The tensile strain in this direction is proportional to the compressive biaxial strain ϵ. The strain tensor corresponding to our situation can therefore be written as

$$\epsilon_{xx}=\epsilon_{yy}=\epsilon,\quad \epsilon_{zz}=-K\epsilon,\quad \epsilon_{xy}=\epsilon_{yz}=\epsilon_{zy}=0\ . \tag{2}$$

Note that in the present experimental configuration, $\epsilon<0$.

Applying boundary conditions and the standard elasticity relations, one obtains

$$K=-\frac{2S_{12}}{S_{11}+S_{12}}\ . \tag{3}$$

Taking the valence-band wave functions in the (J,M_J) representation Eq. (1) can be expressed simply as

$$\begin{aligned}\mathscr{H}_{\text{strain}} = &-(a^c-a^v)(2-K)\epsilon \\ &+3b(1+K)\epsilon(L_z^2-\tfrac{1}{3}L^2)\ , \end{aligned} \tag{4a}$$

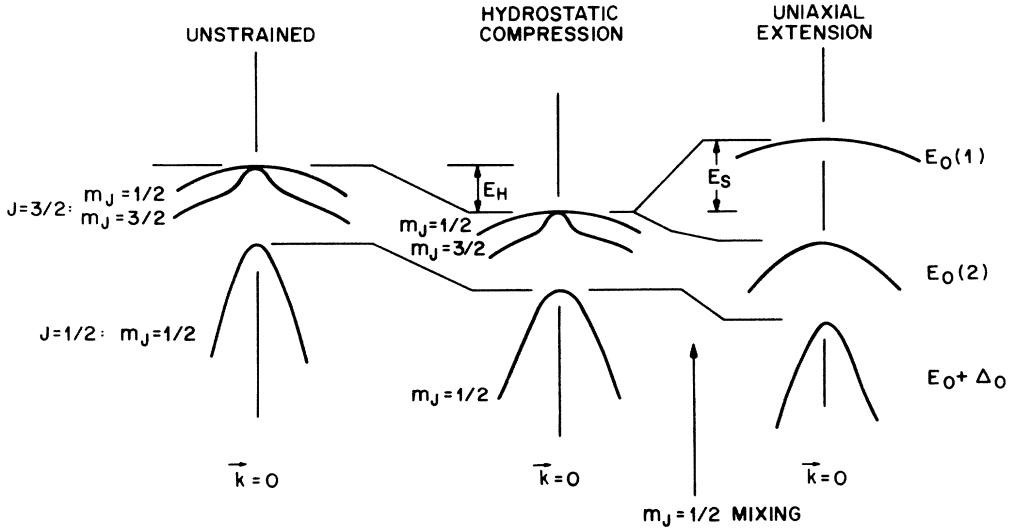

FIG. 4. Schematic diagram of the $J=\frac{3}{2}$ and $J=\frac{1}{2}$ manifolds of the valence band of Ge_xSi_{1-x} alloys. Strain effects push $E_0(1)$ ($|\frac{3}{2},\frac{3}{2}\rangle$) up into the band gap. The strain associated with lattice mismatch causes substantial mixing of the $|\frac{3}{2},\frac{1}{2}\rangle$ and $|\frac{1}{2},\frac{1}{2}\rangle$ bands, tending to drive them apart.

and the Hamiltonian matrix of Eq. (1) becomes[16–19]

$$\mathscr{H}_{ij}=\begin{bmatrix} |\frac{3}{2},\frac{3}{2}\rangle & |\frac{3}{2},\frac{1}{2}\rangle & |\frac{1}{2},\frac{1}{2}\rangle \\ -E_H-E_S & 0 & 0 \\ 0 & -E_H+E_S & E_S\sqrt{2} \\ 0 & E_S\sqrt{2} & -E_H-\Delta_0 \end{bmatrix}, \quad (4b)$$

where Δ_0 is the spin-orbit splitting. The other quantities in Eq. (4) are given by

$$E_H=(a^c-a^v)(2-K)\epsilon\,, \quad (5a)$$

$$E_S=b(1+K)\epsilon\,. \quad (5b)$$

The energy shifts can be calculated to yield

$$\delta E_0(1)=E_H+E_S\,, \quad (6a)$$

$$\delta E_0(2)=E_H+\frac{\Delta_0}{2}-\frac{E_S}{2}-\tfrac{1}{2}(\Delta_0^2+2\Delta_0E_S+9E_S^2)^{1/2}\,, \quad (6b)$$

$$\delta E_0+\Delta_0=E_H+\frac{\Delta_0}{2}-\frac{E_S}{2}+\tfrac{1}{2}(\Delta_0^2+2\Delta_0E_S+9E_S^2)^{1/2}\,. \quad (6c)$$

Since J does not remain a good quantum number, we shall use the designation $E_0(1)$, $E_0(2)$, and $E_0+\Delta_0$ to denote the above features. The uniaxial deformation potential b has been measured for both Si (Refs. 16 and 17) and Ge (Ref. 18). The elastic compliance constants S_{ij} at 300 and 77 K can be obtained from the Landolt-Börnstein tables.[20]

Equations (6a)—(6c) are evaluated as a function of alloy content taking $\epsilon_{xx}=\epsilon_{yy}=\Delta a_0/a_0$ and is negative for the compressive lattice mismatch strain of GeSi alloys grown on Si. This implies E_S is negative and that the $E_0(1)$ state is split upwards while the $E_0(2)$ state is pushed down toward the spin-orbit state, $E_0+\Delta_0$. The hydrostatic shift E_H is divided between the valence band and conduction band. Although Gourley and Biefeld[21] have considered similar strain effects in GaAs-GaAs$_{1-x}$P$_x$ strained-layer superlattices, their work does not include the important coupling between the $|\frac{3}{2},\frac{1}{2}\rangle$ and $|\frac{1}{2},\frac{1}{2}\rangle$ states, even though the magnitude of strain is similar to that encountered in the present work. We note that roughly 50% of the energy shift of the $|\frac{1}{2},\frac{1}{2}\rangle$ state comes from this mixing effect.

Both theoretical and experimental determinations[22–25] of the appropriate deformation potentials indicate that 80% of the hydrostatic shift occurs in the conduction band. This feature means that the hydrostatic shift in the valence band is much smaller than the splitting term. Hence the state under uniaxial tension moves upwards in energy, relative to the top of the valence band in unstrained material, into the gap. In addition, the $\langle 100\rangle$ conduction-band minima are split by the [001] strain, leading to a shrinkage of the indirect gap as a function of strain, even though the effect of the direct gap is opposite. These features of the valence bands are diagramed in Fig. 5. Note that in Fig. 5 the shift of $E_0(1)$ is not linear in alloy content even though it is linear in ϵ [see Eq. (6a)].

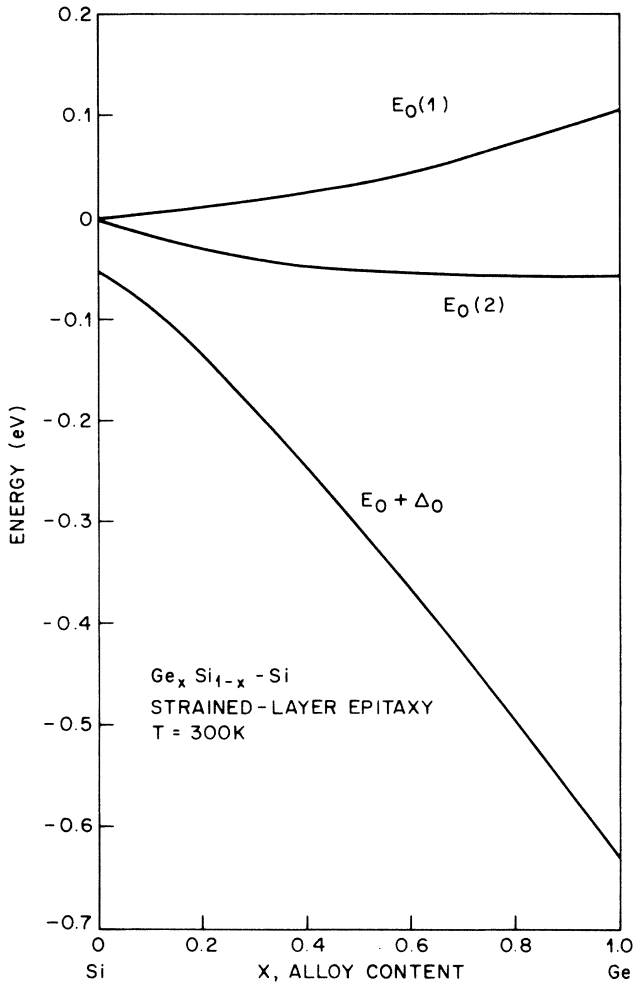

FIG. 5. Strain-induced shifts of the valence bands in Ge_xSi_{1-x} alloys, as a function of alloy content. In preparing this diagram, it is assumed that all of the lattice-mismatch strain is confined to the alloy material. The effects of one-dimensional quantum confinement are not included in this diagram. We have used the results of Refs. 15—18 to divide the total hydrostatic shift between the conduction and valence bands.

This is a consequence of the alloy dependence of the deformation potential b.

B. E_1 and $E_1+\Delta_1$ transitions

The E_1 and $E_1+\Delta_1$ optical features are produced by transitions which occur along the eight equivalent $\langle 111\rangle$ directions (Λ_3-Λ_1) of the Brillouin zone. The strain in this experiment does not remove the degeneracy of these states (i.e., no interband splitting) but does cause an intraband effect, i.e., a stress-induced splitting of the Λ_3 orbital bands.[18]

It has been shown that the effect of a [001] strain on E_1 and $E_1+\Delta_1$ can be expressed as[18]

$$\delta(E_1)=E_H+\tfrac{1}{2}\Delta_1-[(\tfrac{1}{2}\Delta_1)^2+(E_J\pm E_S)^2]^{1/2}\,, \quad (7a)$$

$$\delta(E_1+\Delta_1)=E_H+\tfrac{1}{2}\Delta_1+[(\tfrac{1}{2}\Delta_1)^2+(E_J\pm E_S)^2]^{1/2}\,, \quad (7b)$$

where in our case

$$E_H=\frac{D_1^1}{\sqrt{3}}(2-K)\epsilon\ , \tag{8a}$$

$$E_S=\frac{(\frac{2}{3})^{1/2}}{2}D_3^3(1+K)\epsilon\ , \tag{8b}$$

and D_1^1 and D_3^3 are one-electron deformation potentials. Both of these parameters have been evaluated for Ge (Ref. 18) and Si (Ref. 26).

In Eqs. (7c) and (7b), E_J is a spin-exchange splitting term which has been evaluated to be about 2—4 meV in Ge,[18] but not observed in Si.[26] This quantity is small compared to the E_S in this experiment and hence will be neglected.

It can be shown from Eqs. (7) and (8) that for the strain conditions of this experiment the shift of E_1, i.e., δE_1, is quite small. Therefore, we expect to observe this feature in the quantum-well structures at about the same energy as in the corresponding bulk alloy.

IV. EFFECTS OF QUANTUM CONFINEMENT

As is well known, the effect of spatial confinement of both electrons and holes is to shift the transition energies upward. Since the magnitudes of the shift depends on the effective mass of the carrier involved, quantum effects also serve to lift the degeneracy of the valence-band edge. This effect is seen in the E_0 transition considered in this paper. For the E_1 transition, the confinement effects are relatively small because of the low confinement energies and large masses.[10,12]

The electron and hole confinement energies for the transition discussed in this paper have been determined from the Shubnikov—de Haas experiments of People *et al.* on n^+-n heterojunctions which showed negligible band offset between the $\langle 100\rangle$ conduction-band minima in Si and the Ge_xSi_{1-x} alloys.[27] Therefore, at $\mathbf{k}=0$, 80% of the energy discontinuity for the E_0 transition occurs in the conduction band at Γ. This is consistent with some recent theoretical calculations.[28]

The energy-level picture for the strained quantum well is shown in Fig. 6 for the E_0 transitions for the upper valence bands. As an example, we consider the composition $x=0.65$, corresponding to one of the samples used in our experiments. In the valence band, the confining potential depends on the state involved. Using the results of the preceding section, holes (heavy) in the uppermost state $E_0(1)$ see the full valence-band offset plus the strain splitting giving a confinement potential of 0.4 eV. Holes (light) in the $E_0(2)$ state see essentially only the valence-band offset of 0.28 eV. Because the spin-orbit splitting is so small in Si, there is no confinement for holes in the $E_0+\Delta_0$ band under any conditions of this experiment.

The electrons at E_0 would see a confinement potential corresponding to the remainder of the band offset of 1.82 eV in an unstrained alloy. However, recall that the bulk (80%) of the hydrostatic shift in the E_0 gap occurs through upward shift of the conduction band. This increase reduces the confinement energy to 1.6 eV.

The quantum confinement energies are calculated from

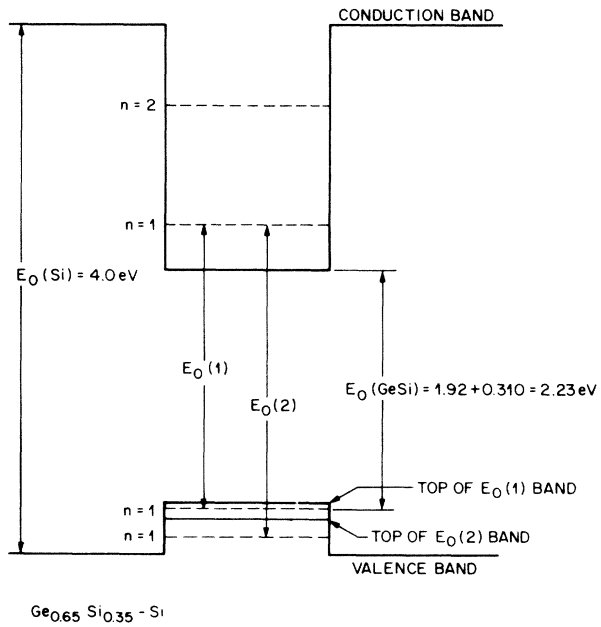

FIG. 6. Quantum shifts in strained-layer wells of Ge_xSi_{1-x} for compositions near $x=0.5$, the effects of strain and quantum confinement become comparable for well thicknesses less than 50 Å. The $J=\frac{3}{2}$ energy surfaces at $\mathbf{k}=0$ are no longer warped but consist of two ellipsoids, one obsolate and the other prolate with respect to the strain axis which is parallel to the confinement direction in our experiments.

numerical solution of the Schrödinger equation for an electron in a one-dimensional potential:

$$\cos(qd)=\cos[\alpha(d-s)]\cosh(\beta s)+\left[x+\frac{1}{x}\right]\sin[\alpha(d-s)]\sinh(\beta s)\ , \tag{9}$$

where d is the superlattice period and s the barrier width,

$$x=\frac{m_b^*}{m_w^*}\frac{\beta}{\alpha}\ ,$$

$$\alpha=\frac{1}{\hbar}(2m_b^*E)^{1/2}\ ,$$

$$\beta=\frac{1}{\hbar}[2m_w^*(V_0-E)]^{1/2}\ ,$$

with m_b^* the effective mass in Si and m_w^* the effective mass in Ge_xSi_{1-x} following the method of Bastard,[29] where continuity of the wave function and continuity of wave-particle current are maintained at the heterointerface.

While the conduction band at Γ is nondegenerate, the valence band is split by the uniaxial component of the strain tensor, resulting in two ellipsoidal energy surfaces. The appropriate effective mass component to be used in the calculation of confinement energies is the effective mass in the superlattice direction, perpendicular to the layer planes. For the particular strain configuration of our experiments, this mass component lies along a direction parallel to the strain axis. The appropriate masses

for the two valence bands are easily calculated using the Hensel formulation:[16]

$$\frac{m}{m_{||}}=(A-B)=-4.09, \quad \frac{m_{||}}{m_0}=0.244 \tag{10a}$$

for the uppermost band, $E_0(1)$, and

$$\frac{m}{m_{||}}=(A+B)=-13.47, \quad \frac{m_{||}}{m_0}=0.074 \tag{10b}$$

for the valence band, $E_0(2)$, where we have used interpolated parameters for a $Ge_{0.5}Si_{0.5}$ alloy.

In this paper only the quantum shifts at the E_0 transition are treated in our analysis because it is the only optical transition for which the effective-mass parameters are sufficiently well-known in both valence and conduction bands. Our results show that quantum shifts at the E_1 transitions are only about 20% as large as those measured at E_0. At E_2 there is no quantum shift at all because the confining potential is negligible for all alloy compositions as can be seen in Fig. 3.

V. EXPERIMENTAL RESULTS

In Figs. 7(a) and 7(b) we show the direct experimental trace of a multiple-quantum-well structure containing 75-Å-thick wells of $Ge_{0.45}Si_{0.55}$ sandwiched between 275-Å Si confinement barriers at 300 and 77 K, respectively. This structure contains 20 periods, or a total alloy thickness of 1500 Å. Reference to Fig. 3 shows that all structure from the Si barrier layers is confined to energies greater than 3.3 eV. The features denoted E_0'(Si) and E_1(Si) are signals from the Si confinement layers.

The electroreflectance features from the quantum-well structures occur at energies below 3.3 eV and are denoted by A, B, C, and D. The E_0 band gap in unstrained alloys of this composition is at 2.4 eV at room temperature (see Fig. 3), and absence of any structure at this energy in Fig. 7(a) shows clearly that strains and confinement have pushed the transitions to higher energies. We identify feature A with the $E_0(1)$ and $E_0(2)$ quantum-well transitions.

Comparison of Figs. 7(a) and 7(b) shows that the temperature shift for all transitions appears to be uniform, corresponding closely to the value of 4×10^{-4} eV/K. In addition, the transition linewidths have been reduced sufficiently to resolve clearly the E_1,E_0' of the Si barrier layers. However, the splitting of the $J=\frac{3}{2}$ state ≈ 80 meV for $x=0.45$ (see Fig. 5) is still not resolved at 77 K.

In Fig. 8 we show a micrograph of the actual quantum-well structure of our second sample containing 65 at. % Ge and 35 at. % Si. This enlargement of the micrograph on the right-hand side was made using a multiple-beam technique allowing resolution of the atomic positions. There are no dislocations at the interfaces which can be confirmed by tilting the photograph and sighting along atomic planes. However, the strain in the $Ge_{0.65}Si_{0.35}$ layer is easily distinguished by the jog in the atomic planes at the interfaces. Alloy disorder and other effects create an interface thickness of about 3 atomic layers, or 10% of the quantum-well thickness. This uncertainty contributes to the width of the spectra both from strain and quantum effects.

Shown in Figs. 9(a) and 9(b) are the ER spectra at 300 K and 77 K, respectively, of a multiple-quantum-well structure containing 33-Å-thick wells of $Ge_{0.65}Si_{0.35}$. The lattice-mismatch strain in this sample is 2.6% versus 1.8% for the $Ge_{0.45}Si_{0.55}$ sample in Figs. 7(a) and 7(b). In order to obtain commensurate strained epitaxy, the alloy thickness must be reduced by about 50% to 33 Å. Twenty periods of alloy and confinement layers were grown in this sample. The total alloy thickness is therefore only 660 Å for this structure.

The features arising from the Si cladding layers are denoted E_0'(Si) and E_1(Si) in Figs. 9(a) and 9(b). For this alloy composition E_0 of the bulk material should occur around 2 eV (see Fig. 3), and clearly there is no structure

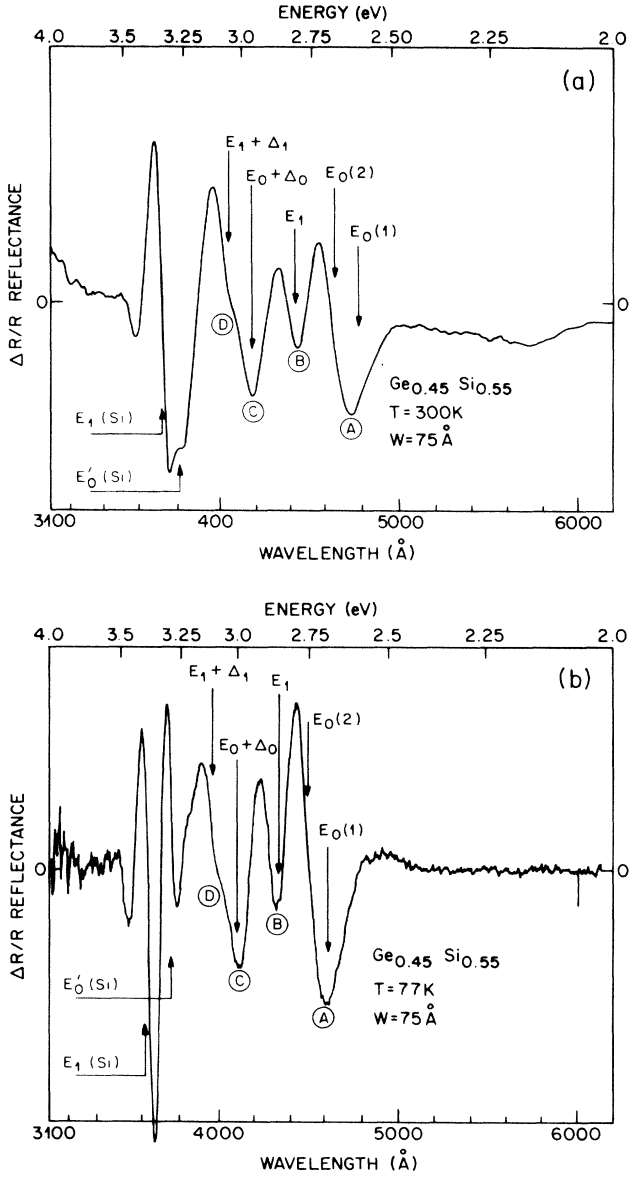

FIG. 7. Electroreflectance spectrum of $Ge_{0.45}Si_{0.55}$ taken at (a) 295 K and (b) 77 K. These spectra show signals from the Si barriers as well as the $Ge_{0.45}Si_{0.55}$ quantum wells which are 75 Å thick. Quantum confinement shifts in this sample are second-order effects compared to strain because of the well width.

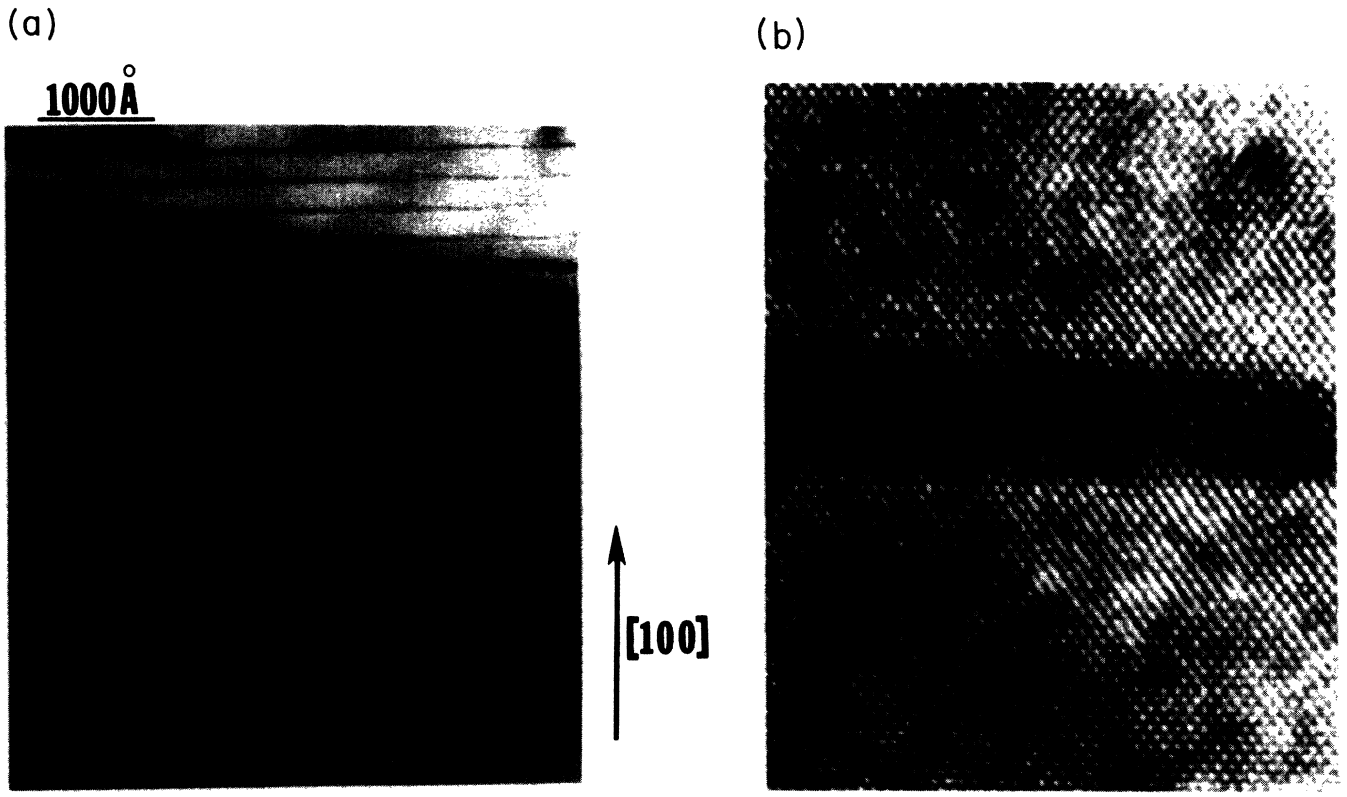

FIG. 8. Phase contrast transmission electron micrograph of 33-Å-wide quantum-well structure demonstrating continuity of layers, absence of dislocations, and relative smoothness of layers.

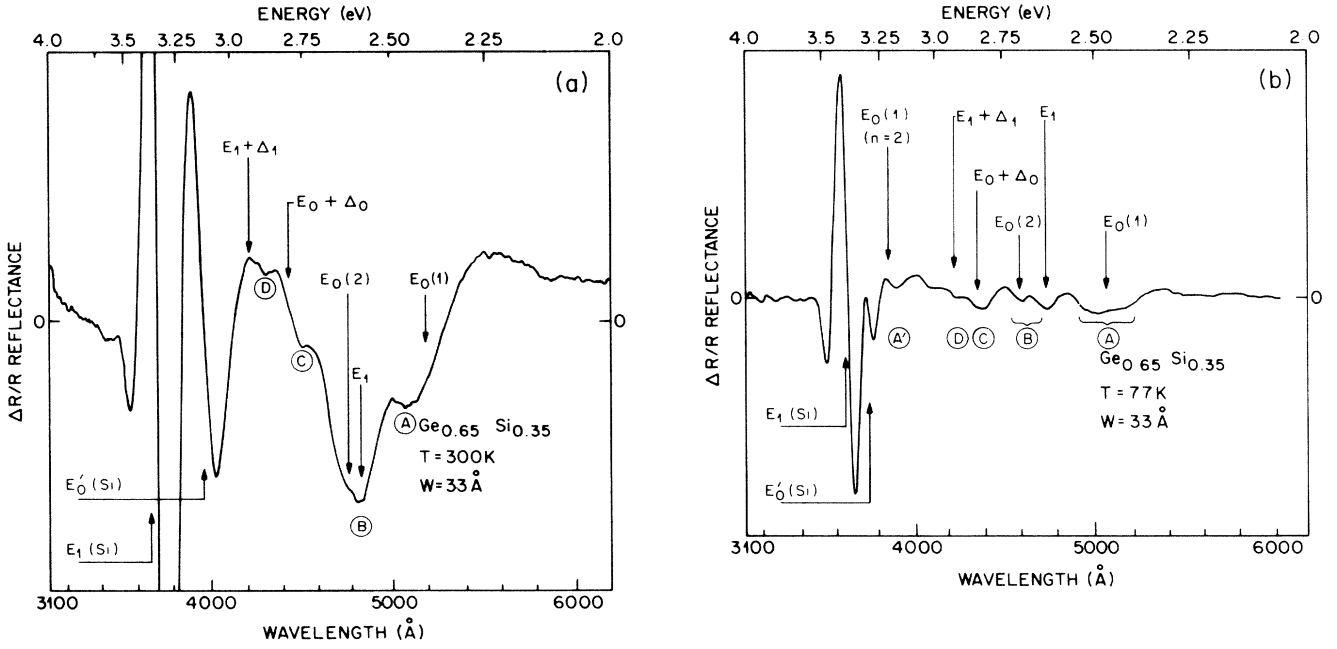

FIG. 9. Electroreflectance spectra of the $Ge_{0.65}Si_{0.35}$ multiple-quantum-well sample shown in Fig. 8 at (a) 295 K and (b) 77 K. The alloy reflectance signal comes from only 20 wells, or a total thickness of $\approx$660 Å.

in this range. In Fig. 9(a) the features from the quantum wells are denoted A, B, C, and D. This relatively narrow well produces a quantum splitting of the E_0 level which is so large that $E_0(2)$, the "light-hole" transition, occurs higher in energy than the E_1 transition. The 77-K spectra are quite rich and contain eight spectral features which are labeled A, B, C, D, and A', with A and B being doublets.

VI. INTERPRETATION OF EXPERIMENTAL RESULTS

A. E_0, $E_0+\Delta_0$ features

The effects of strain and electron and hole confinement for $E_0(1)$, $E_0(2)$, and $E_0+\Delta_0$ are summarized in Tables I and II for the $x=0.45$ and 0.65 structures, respectively, at both 300 and 77 K. Solution of Eq. (8) yields a quantum shift for the electrons at E_0 of 0.05 eV for the 75-Å well and 0.22 eV for the 33-Å well ($n=1$ levels). Because of the substantially larger mass of holes and small offset in the valence band, for the 75-Å well there is essentially no hole confinement while for the 33-Å wells the hole ground-state energies are shifted for $E_0(1)$ and $E_0(2)$ by 50 and 90 MeV, respectively. As discussed above the holes in $E_0(1)$ are confined by a larger potential than those of $E_0(2)$. The mass along the quantum potential (i.e., [001]) is greater for the former in relation to the latter, which increases the total splitting between these two levels to about 220 meV. For $E_0+\Delta_0$ there is no confinement at either temperature.

It is clear from Tables I and II that the A features in Figs. 7(a) and 7(b) are associated with $E_0(1)$ and $E_0(2)$, respectively. For the $x=0.45$ wells this splitting (≈ 80 meV) is too small to be resolved at either 300 or 77 K. However, for the $x=0.65$ structures this splitting is resolved at both 300 and 77 K and is responsible for the doublet nature of B in Figs. 9(a) and 9(b). The B feature in the spectra of Figs. 9(a) and 9(b) is composed of the $E_0(2)$ transition and E_1 transition (which is discussed below). The separation of this doublet from the A doublet is about 220 meV, in good agreement with the calculated separation of $E_0(1)$ and $E_0(2)$ listed in Table II. The energy position of $E_0(1)$ and $E_0(2)$ at about 2.4–2.5 eV at 300 K for $x=0.65$ is in general agreement with the resonant Raman experiment of Cerdeira *et al.*,[9] but the superior definition of the ER data makes resolution of each component clear for the first time.

In the above figures we have indicated the position of $E_0+\Delta_0$ from Tables I and II. It can be seen that $E_0+\Delta_0$ corresponds to feature C in the ER spectra of both quantum-well systems.

The feature marked A' in Fig. 9(b) corresponds to the $n=2$ $E_0(1)$ and $E_0(2)$ quantum transitions. Solution of Eq. (8) for $E_0(1)$ yields a total quantum shift of the electrons of 890 meV for this transition [however, the $n=2$ transition for $E_0(2)$ is buried in the E_1 and E_0' peaks for Si]. For the $x=0.65$ structures, the calculated energies of the $n=2$ $E_0(1)$ and $E_0(2)$ features are 3.254 and 3.483 eV at 77 K. The $E_0(1)$, $n=2$ transition is observed at 3.24 eV in fair agreement with calculation.

B. E_1, $E_1+\Delta_1$ features

The effects of strain on E_1 and $E_1+\Delta_1$ for $x=0.45$ and $x=0.65$ structures also are listed in Tables I and II,

TABLE I. Comparison of calculated and measured transition energies for the Si-$Ge_{0.45}Si_{0.55}$ quantum wells studied in this work at 300 and 77 K. $x=0.45$. (conf. denotes confinement.)

Temperature (K)	Transition	E_0	Strain shift	Electron conf.	Hole conf.	Calc.	Measured
300	$E_0(1)$	2.40[a]	+0.144	+0.05	+0.0	2.594	2.610
	$E_0(2)$	2.40[a]	+0.223	+0.05	+0.0	2.673	
	$E_0+\Delta_0$	2.40+0.160[a]	+0.300	+0.05	+0.0	2.910	2.950
Temperature (K)	Transition	E_1	Strain strain	Electron conf.	Hole conf.	Calc.	Measured
300	E_1	2.77[a]	+0.016	+0	+0	2.793	2.80
	$E_1+\Delta_1$	2.777+0.106[a]	+0.21	+0	+0	3.097	3.10
Temperature (K)	Transition	E_0	Strain shift	Electron conf.	Hole conf.	Calc.	Measured
77	$E_0(1)$	2.49[b]	+0.144	+0.05	+0.0	2.684	2.740
	$E_0(2)$	2.49[b]	+0.223	+0.05	+0.0	2.763	
	$E_0+\Delta_0$	2.49+0.160[b]	+0.300	+0.05	+0.0	3.000	3.062
Temperature (K)	Transition	E_1	Strain shift	Electron conf.	Hole conf.	Calc.	Measured
77	E_1	2.867[b]	+0.016	+0	+0	2.883	2.85
	$E_1+\Delta_1$	2.877+0.106[b]	+0.214	+0	+0	3.187	3.10

[a]From Ref. 15.

[b]Based on a temperature coefficient of 4×10^{-4} eV/K.

TABLE II. Comparison of calculated and measured energies for the Si-$Ge_{0.65}Si_{0.35}$ quantum wells studied in this work at 300 and 77 K. NO denotes not observed; NC denotes not confined. $x=0.65$.

Temperature (K)	Transition	E_0	Confinement Strain	Confinement Electron	Confinement Hole	Calc.	Measured
300	$E_0(1)$, $n=1$	1.92[a]	+0.204	+0.22	+0.04	2.384	2.40
	$E_0(2)$, $n=1$	1.92[a]	+0.313	+0.22	+0.10	2.553	2.61
	$E_0+\Delta_0$, $n=1$	1.92+0.210[a]	+0.449	+0.22	NC	2.799	2.75
	$E_0(1)$, $n=2$	1.92[a]	+0.204	+0.890	+0.16	3.174	NO
	$E_0(2)$, $n=2$	1.92[a]	+0.313	+0.890	NC	3.403	NO
Temperature (K)	Transition	E_1	Strain	Electron	Hole	Calc.	Measured
300	E_1	2.50[a]	+0.013	+0	+0	2.513	2.55
	$E_1+\Delta_1$	2.520+0.140[a]	+0.313	+0	+0	2.973	2.90
Temperature (K)	Transition	E_0	Strain	Electron	Hole	Calc.	Measured
77	$E_0(1)$, $n=1$	2.01[b]	+0.204	+0.22	+0.040	2.474	2.46
	$E_0(2)$, $n=1$	2.01[b]	+0.313	+0.22	+0.10	2.643	2.68
	$E_0+\Delta_0$, $n=1$	2.01+0.210[b]	+0.449	+0.22	NC	2.889	2.82
	$E_0(1)$, $n=2$	2.01[b]	+0.204	+0.890	+0.160	3.264	3.21
	$E_0(2)$, $n=2$	2.01[b]	+0.313	+0.890	NC	3.493	NO
Temperature (K)	Transition	E_1	Strain	Electron	Hole	Calc.	Measured
77	E_1	2.610[b]	0.313	+0	+0	2.623	2.61
	$E_1+\Delta_1$	2.610+0.140[b]	+0.313	+0	+0	3.063	2.92

[a]From Ref. 15.
[b]Based on temperature coefficient of 4×10^{-4} eV/K.

respectively, at 300 and 77 K. For this transition the electron and hole confinement are negligible because of the heavy masses and relatively small band offsets. The E_1 feature does not shift very much for the strains in this experiment. Thus it is clear from Figs. 7(a), 7(b), 9(a), and 9(b) that the principal part of the peak labeled *B* originates from the E_1 transition [in Figs. 9(a) and 9(b), the *B* feature contains an additional feature due to $E_0(2)$ as discussed above]. From Tables I and II the shift of $E_1+\Delta_1$ is 0.30 eV ($x=0.45$) and 0.44 eV ($x=0.65$). Thus, the *D* feature in the above figures corresponds to $E_1+\Delta_1$.

The origin of the doublet nature of *A* seen in the data of Figs. 9(a) and 9(b) is not completely understood at this time. Further studies on samples of similar structure and compositions are underway to clarify this point.

VII. CONCLUSIONS

The excellent agreement between the theoretical framework and experiment as shown in Tables I and II is significant in several respects. The presence of strain which is quantitatively measured in these spectra confirms that commensurate strained-layer epitaxy can be achieved in Ge_xSi_{1-x} alloys grown on Si with substantial Ge content. The strain-induced coupling between $|\frac{3}{2},\frac{1}{2}\rangle$ and $|\frac{1}{2},\frac{1}{2}\rangle$ must be taken into account to obtain accurate results.[21] The formation of lattice-mismatch dislocations would reduce the strain and the strain-associated shift in the transition energies. The close agreement between calculated and measured transition energies indicated an insignificant concentration of misfit dislocations. The accurate accounting for quantum shifts of both electron and hole states lends strong support to the band lineup between Si and Ge_xSi_{1-x} alloys deduced from Shubnikov–de Haas measurements[27] and recent theoretical calculations.[28]

Finally, because the epitaxy of Ge_xSi_{1-x} on Si requires the growth of multiple-quantum-well structures, these measurements provide the first quantitative data on both the E_0 and E_1 optical transition energies in these strained-layer structures as a function of composition. It also demonstrates that modulation spectroscopy is a powerful tool for studying quantum wells and superlattices.

ACKNOWLEDGMENTS

The authors wish to thank D. Aspnes, F. Cerdeira, J. C. Hensel, R. M. Martin, P. Parayanthal, R. People, A. Pinczuk, and B. Wilson for many fruitful discussions concerning these experiments. One of us (F.H.P.) wishes to acknowledge the support of the New York State Foundation for Science and Technology as part of its Centers in Advanced Technology Program.

*Present address: Hewlett-Packard Laboratories, Palo Alto, CA 94304.

[1]J. C. Bean, J. Vac. Sci. Technol. A **1**, 540 (1983).

[2]B. A. Joyce, Rep. Prog. Phys. **37**, 363 (1974).

[3]Y. Ota, Thin Solid Films **106**, 1 (1983).

[4]J. C. Bean, L. C. Feldman, A. T. Fiory, S. Nakahara, and I. K. Robinson, J. Vac. Sci. Technol. A **2**, 436 (1984).

[5]H. M. Manasevit, I. S. Gergis, and A. B. Jones, Appl. Phys. Lett. **41**, 464 (1982).

[6]J. A. Moriatry and S. Krishnamurthy, J. Appl. Phys. **54**, 1892 (1983).

[7](a) T. P. Pearsall and J. C. Bean, IEEE Electron Devices Lett. (to be published); (b) T. P. Pearsall, H. Temkin, N. A. Olsson, and S. Luryi, IEEE Electron Devices Lett. (to be published).

[8]F. Cerdeira, A. Pinczuk, J. C. Bean, B. A. Batlogg, and B. A. Wilson, Appl. Phys. Lett. **48**, 1138 (1984).

[9]F. Cerdeira, A. Pinczuk, and J. C. Bean, Phys. Rev. B **31**, 1202 (1985).

[10]E. E. Mendez, L. L. Chang, G. Lundgren, R. Ludeke, L. Esaki, and F. H. Pollak, Phys. Rev. Lett. **46**, 1230 (1981).

[11]O. J. Glembocki, B. V. Shanabrook, N. Bottka, W. T. Beard, and J. Comas, *Proceedings of the Society of Photo-optical Instrumentation Engineers* (SPIE, Bellingham, 1985), Vol. 524, p. 86; O. J. Glembocki, B. V. Shanabrook, N. Bottka, W. T. Beard, and J. Comas, Appl. Phys. Lett. **46**, 970 (1985).

[12]M. Erman, J. B. Theeten, P. Frijlink, S. Gaillard, F. J. Hia, and C. Alibert, J. Appl. Phys. **56**, 3241 (1984).

[13]J. C. Bean and E. A. Sadowski, J. Vac. Sci. Technol. **20**, 137 (1982).

[14]See, for example, D. E. Aspnes, in *Handbook on Semiconductors*, edited by M. Balkanski (North-Holland, New York, 1980), Vol. 2, p. 109.

[15]J. S. Kline, F. H. Pollak, and M. J. Cardona, Helv. Phys. Acta **41**, 968 (1968).

[16]J. C. Hensel and G. Feher, Phys. Rev. **129**, 1041 (1963).

[17]L. D. Laude, F. H. Pollak, and M. Cardona, Phys. Rev. B **3**, 2623 (1971).

[18]M. Chandrasekhar and F. H. Pollak, Phys. Rev. B **15**, 2127 (1977).

[19]We have neglected the small effect of the strain dependence of the spin-orbit splitting.

[20]*Physics of Group IV Elements and III-V Compounds*, Vol. 17a of *Landolt-Börnstein*, edited by O. Madelung (Springer-Verlag, Heidelberg, 1982).

[21]T. L. Gourley and R. M. Biefeld, Appl. Phys. Lett. **45**, 749 (1984).

[22]H. Hasegawa, Phys. Rev. **129**, 1029 (1963).

[23]J. C. Hensel and K. Suzuki, Phys. Rev. B **9**, 4219 (1974).

[24]J. A. Verges, D. Glotzel, M. Cardona, and O. K. Andersen, Phys. Status Solidi B **113**, 519 (1982).

[25]R. M. Martin and C. G. Van de Walle, Bull. Am. Phys. Soc. **30**, 226 (1985).

[26]G. W. Rubloff and F. H. Pollak, Phys. Rev. Lett. **29**, 789 (1972).

[27]R. People, J. C. Bean, D. V. Lang, A. M. Sergent, H. L. Störmer, K. W. Wecht, R. T. Lynch, and K. Baldwin, Appl. Phys. Lett. **45**, 1231 (1985).

[28]C. G. Van de Walle and R. M. Martin, Bull. Am. Phys. Soc. **30**, 226 (1985); J. Vac. Sci. Technol. (to be published).

[29]G. Bastard, Phys. Rev. B **24**, 5693 (1981).

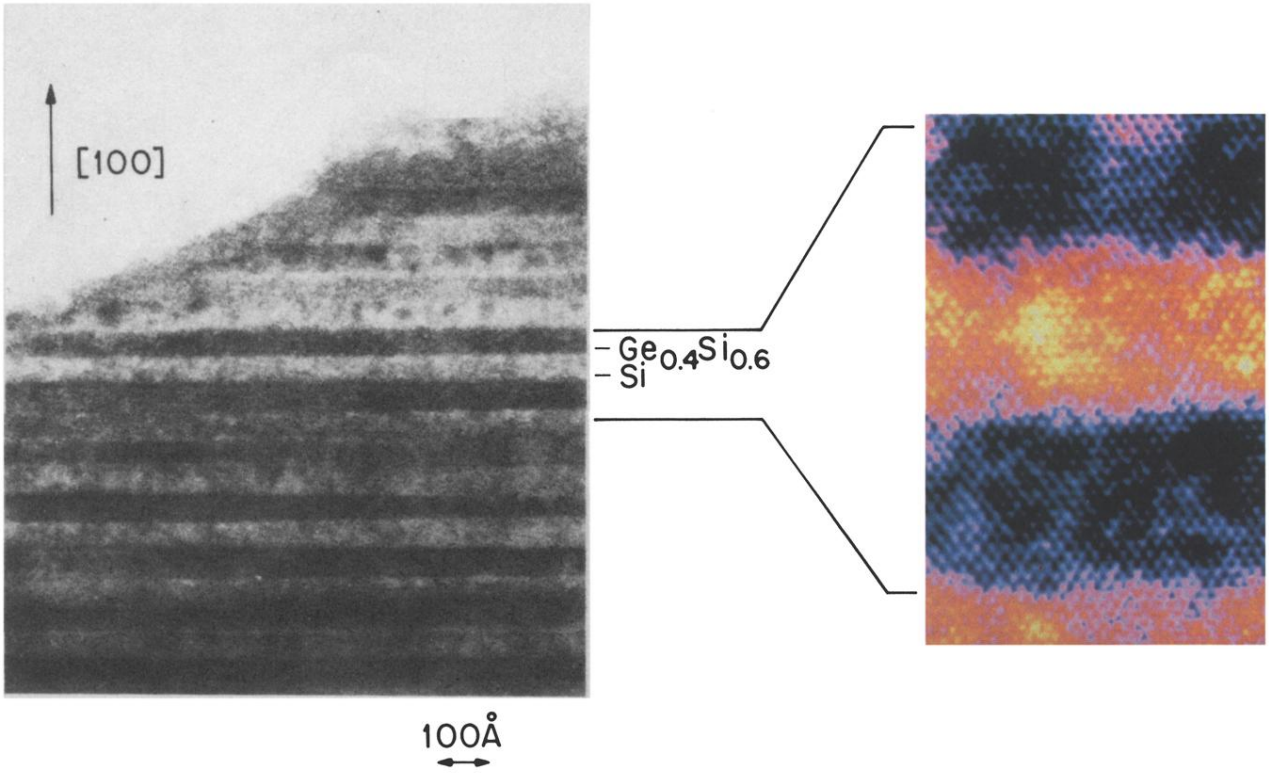

FIG. 2. Transmission electron micrographs of a typical strained-layer superlattice. Left-hand photo: cross section of entire structure. Right-hand photo: phase contrast image resolving atomic pairs. Image has been computer color enhanced to expand contrast scale.

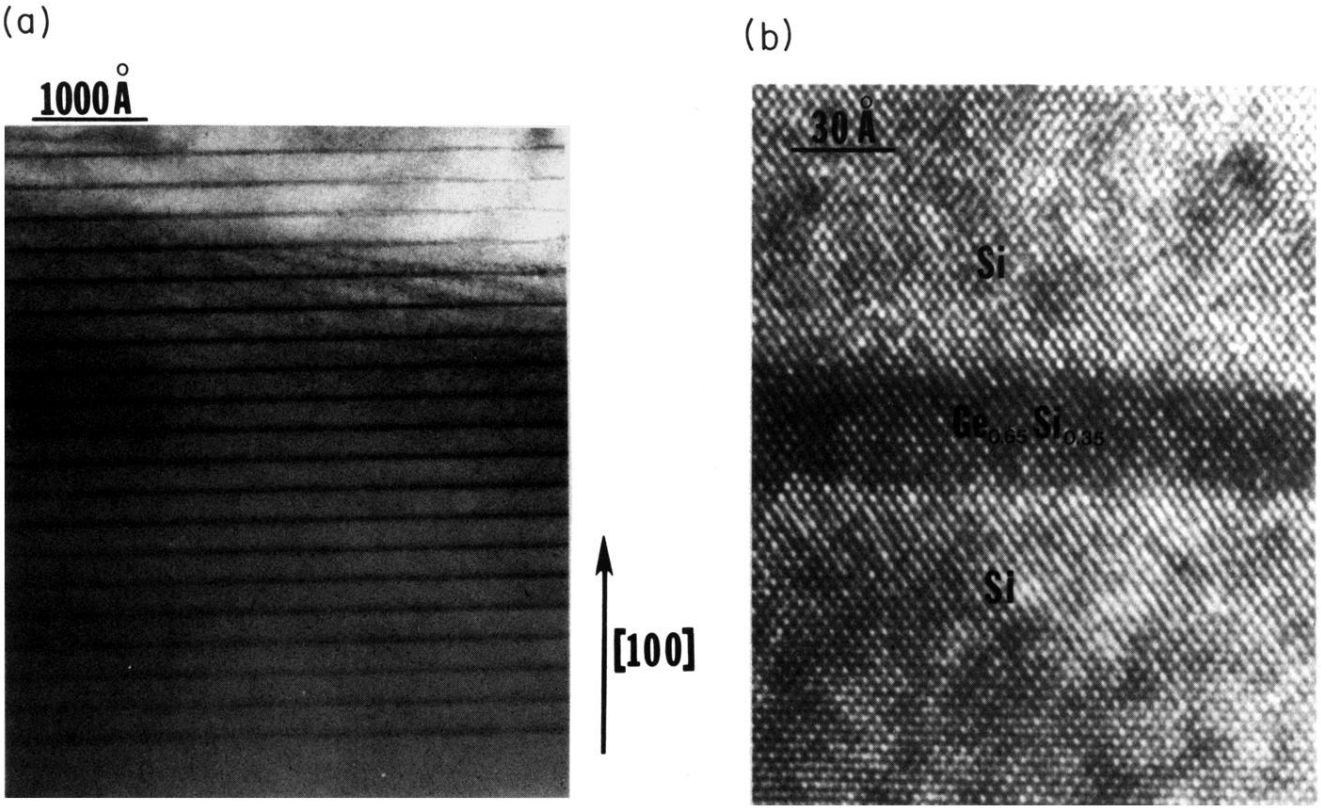

FIG. 8. Phase contrast transmission electron micrograph of 33-Å-wide quantum-well structure demonstrating continuity of layers, absence of dislocations, and relative smoothness of layers.